NIPPON STEEL TECHNICAL REPORT No. 136 JULY 2026

Technical Report

X-ray Line Profile Analysis by Micro-focus XRD

Atsuhiro ITOH* Muneyuki IMAFUKU

Abstract

X-ray Line Profile Analysis (XLPA) is a powerful and convenient method to investigate dislocation density, crystallite size and nature (screw or edge), and arrangement of dislocation in a material. However, few studies have been conducted concerning the application limit of dislocation density measurements for localized regions or curved materials. In this study, X-ray diffraction measurements of iron powders formed into flat plates and cylinders were performed using the micro-focus method, and XLPA was performed. The result revealed that almost the same dislocation density as that of the Bragg-Brentano method could be derived for the flat specimen by the micro-focus method, and the dislocation density of the cylindrical specimen was almost the same as that of the flat specimen up to a radius of 10 mm.

1. Introduction

Dislocations possess diverse properties, such as altering the mechanical strength of metallic materials and the diffusion rate of atoms, and serving as nucleation sites for precipitates. Therefore, techniques for accurately measuring dislocation density are required in various fields for materials development.

The standard quantitative method for dislocation density is direct observation using Transmission Electron Microscopy (TEM). However, it is difficult to achieve accurate quantification in materials with high dislocation density due to the overlap of dislocations. In contrast, X-Ray Diffraction (XRD) quantifies dislocation density changes based on the width and shape of diffraction peaks, making it suitable for materials with high dislocation densities. The XRD technique for quantifying dislocation density is called X-ray Line Profile Analysis (XLPA). Since the 1950s, two methods have existed and been used for XLPA: the Williamson-Hall method,[1] which uses the integral breadth or peak width at half maximum, and the Warren-Averbach method,[2] which uses Fourier coefficients of peak profiles. However, both methods suffered from significant errors due to the anisotropy of strain in metals (the property where the amount of strain varies depending on the crystal orientation).

Amidst this situation, in the 1990s, Ungár et al. proposed new methods—modified Williamson-Hall and modified Warren-Averbach methods[3–5]—that takes into account strain anisotropy for the analysis. This enabled accurate measurement of dislocation density and crystallite size in steel materials using XRD. Furthermore, in recent years, the Convolutional Multiple Whole Profile (CMWP) method, which fits the entire profiles of numerous X-ray peaks simultaneously, has also begun to be used in synchrotron radiation and neutron analysis.[6] These new methods enable the evaluation of not only dislocation density and crystallite size but also previously unattainable parameters such as the presence or absence of dislocation cell formation and the fraction of screw and edge dislocations.

XLPA requires precise peak profiles, necessitating the use of high-angle-resolution optics known as the Bragg-Brentano (B-B) method and a flat measurement surface area of approximately 1–2 cm square. Consequently, it is difficult to apply XLPA to small specimens for micro-tensile test or thermo-mechanical simulator, or to curved sections such as wires or torsion specimens. While synchrotron radiation is suitable for measuring small specimens due to its extremely fine beam diameter and high intensity, XLPA requires at least several thousand crystal grains within the gauge volume to obtain macroscopic averages. This leads to problems with statistical precision when the beam diameter becomes too close to the grain size.[6]

In contrast, the micro-focus method in the laboratory uses a probe diameter of around 1 mm, resulting in a smaller statistical precision problem compared to synchrotron radiation. However, there are very few cases where XLPA has been applied using the micro-focus method in the laboratory, and its accuracy is uncertain.

Therefore, this study compared XLPA results obtained using the micro-focus method and the B-B method in the laboratory and also examined the limitations of applying it to curved specimens.

First, we investigated methods to calculate the same dislocation

* Dr. Eng., Senior Manager, Structure Characterization Dept., Physical Characterization Solution Div., R&D Supporting Unit, Nippon Steel Technology Co., Ltd. 20-1 Shintomi, Futtsu City, Chiba Pref. 293-0011

density using both micro-focus and B-B methods for flat specimens. Next, for curved specimens, we examined how X-ray peak profiles change with increasing specimen curvature using both measurements and numerical simulations. Finally, we investigated the limitations of applying the micro-focus method to curved specimens.

2. Experiments

2.1 Sample preparation

Iron powder with 99.8 wt% purity, sieved to a particle size of 32 μm or less, was ball-milled. Samples were then molded into flat and hemicylindrical shapes using epoxy resin. The sample shapes and milling times are shown in **Table 1**. Flat denotes flat plate samples, while R5, R10, and R15 denote curved hemicylindrical samples with radii of 5 mm, 10 mm, and 15 mm, respectively.

Table 1 Milling time and shape of samples

Sample name	Milling time / h	Shape
0h-F	0	Flat
0h-R5		R5
0h-R10		R10
0h-R15		R15
1h-F	1	Flat
1h-R5		R5
1h-R10		R10
1h-R15		R15
6h-F	6	Flat
6h-R5		R5
6h-R10		R10
6h-R15		R15

2.2 X-ray diffraction

The X-ray diffraction patterns of the samples listed in Table 1 were collected using cobalt radiation on Rigaku SmartLab diffractometer. For the B-B method, the angles of the divergence slit and scattering slit were 2/3°, the aperture width of receiving slit was 0.3 mm, and the divergence angle of both the incident and detection solar slits was 0.5°. A graphite curved monochromator and a scintillation counter were used as the detector. For the micro-focus method, a multilayer mirror and polycapillary were used on the incident side, with a collimator aperture of 0.2 mmφ. A semiconductor 2D detector was used for θ-2θ measurements. **Figure 1** shows the positional relationship of the curved sample relative to each optical system.

The paper plane depth direction was defined as the x-direction, the diffraction vector as the y-direction, and the X-ray propagation direction when the X-ray incidence angle θ was 0° as the z-direction. For the curved sample, it was positioned so that the axis passing through its center was parallel to the z-direction, and the vertex of the curved surface was adjusted to coincide with the center of the goniometer.

The X-ray peak profiles obtained from the sample corresponded to the diffraction indices hkl=110, 200, 211, 220. After suppressing the CoKα_2 line profile using the Rachinger method[7], the profiles were fitted with Voigt function composed of a convolution of Gaussian and Lorentz functions to determine the full width at half maximum (FWHM) of the Gaussian component (W_G) and the Lorentz component (W_L).

Next, the physical profile required for calculating the dislocation

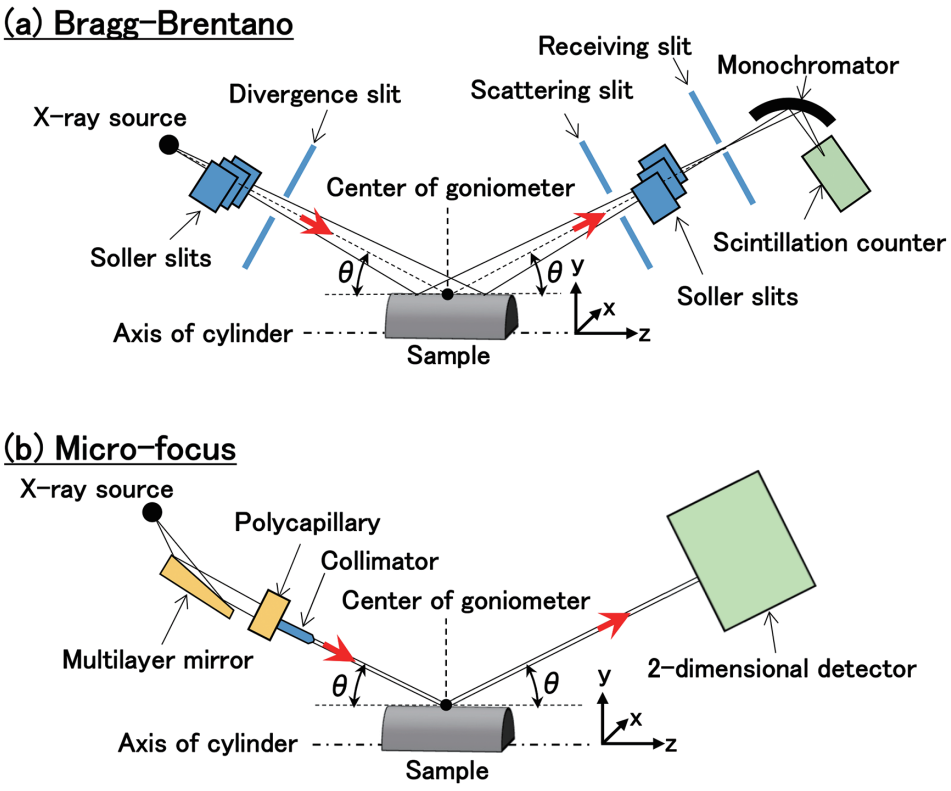

Fig. 1 Schematic diagram of the X-ray diffraction system

density was extracted by deconvolving the peak profile of the sample using the instrumental broadening obtained from the standard sample (NIST LaB_6, SRM 660b) via Equation (1).

$$W_{fG}^2 = W_{hG}^2 - W_{gG}^2 \quad (1a)$$
$$W_{fL} = W_{hL} - W_{gL} \quad (1b)$$

Here, W is the full width at half maximum (FWHM), the subscript G denotes the Gaussian component, and L denotes the Lorentzian component. f indicates the physical profile used for analysis (the sample-derived profile), h denotes the profile obtained from measuring the sample, and g corresponds to the instrument-derived profile obtained from XRD measurement of LaB_6.

In XLPA, since the profile is converted to the reciprocal space before analysis, the peak position 2θ of the physical profile in real space was converted to the peak position $K=2\sin\theta/\lambda$ in the reciprocal space. Furthermore, the peak width $\Delta 2\theta$ in real space was transformed to the reciprocal space using the approximation $\Delta K=(\Delta 2\theta)\cos\theta/\lambda$. Here, θ is half the diffraction angle, and λ is the X-ray wavelength. The unit of $\Delta 2\theta$ was converted from degrees to radians.

2.3 Analysis method

The dislocation density, crystallite size, dislocation arrangement parameters, and screw dislocation fraction were calculated using the modified Williamson-Hall/modified Warren-Averbach method. An overview of the analysis method is shown below.

First, the modified Williamson-Hall method is used to calculate the parameters for correcting strain anisotropy (the average contrast factor) and the fraction of screw dislocations. There are two modified Williamson-Hall equations. The first assumes that both the peak broadening due to crystallite size (W_{size}) and the peak broadening due to lattice distortion ($W_{distortion}$) can be expressed by Lorentz functions. It is derived from the relationship $W=W_{size}+W_{distortion}$ (Equation (2a)). The second assumes they can be expressed by Gaussian functions and is derived from the relationship $W^2=W_{size}^2+W_{distortion}^2$ (2b). Ungár et al.[4] used Equation (2b) to derive Equation (5) described later.

$$\Delta K \cong \frac{k}{\langle t\rangle_{vol}} + \left(\frac{\pi T^2 b^2}{2}\right)^{\frac{1}{2}} \rho^{\frac{1}{2}} \left(K\bar{C}^{\frac{1}{2}}\right) + O\left(K^2\bar{C}\right) \quad (2a)$$

$$\Delta K^2 \cong \left(\frac{k}{\langle t\rangle_{vol}}\right)^2 + \left(\frac{\pi T^2 b^2}{2}\right)\rho\left(K^2\bar{C}\right) + O\left(K^4\bar{C}^2\right) \quad (2b)$$

Here, k is the Scherrer constant, which is 0.9 when using the FWHM of the diffraction peak and 1 when using the integral breadth. Since the integral breadth was used in this experiment, $k=1$. T is a coefficient dependent on the effective cutoff radius R_e of the dislocation, b is the magnitude of the Burgers vector, ρ is the dislocation density, $\bar{C}$ is the average contrast factor, $\langle t\rangle_{vol}$ is the volume-weighted average crystallite size, and O is the higher-order term. For cubic crystals, $\bar{C}$ is expressed by the following equation. h, k, and l are diffraction indices.

$$\bar{C}_{hkl} = \bar{C}_{h00}\left(1 - qH^2\right) \quad (3)$$

$$H^2 = \frac{h^2k^2 + h^2l^2 + k^2l^2}{\left(h^2+k^2+l^2\right)^2} \quad (4)$$

$\bar{C}_{h00}=0.28$ and $q_{edge}=1.29$, $q_{screw}=2.63$ were calculated by inputting the elastic compliance of pure iron into the software ANIZC[8] developed by A. Borbély.

$\bar{C}_{hkl}$ other than $\bar{C}_{h00}$ can be obtained by substituting the values of $\bar{C}_{h00}$ and H^2, along with the experimental value q_{exp}, into Equation (3). The method for calculating the experimental value q_{exp} is shown below. Substituting Equation (3) into Equation (2b), eliminating higher-order terms, and then we get Equation (5).

$$\frac{\Delta K^2 - \alpha}{K^2} \cong \beta\bar{C}_{h00}\left(1 - qH^2\right) \quad (5)$$

$$\beta = \left(\frac{\pi T^2 b^2}{2}\right)\rho,\ \alpha = \left(\frac{1}{\langle t\rangle_{vol}}\right)^2 \quad (6)$$

Since Equation (5) is a linear function with variable H^2, the α value can be determined where the plot of $(\Delta K^2-\alpha)/K^2$ against H^2 lies on a straight line. The reciprocal of the x-intercept then yields the value of q_{exp}. Substituting this value into Equation (7) gives the screw dislocation fraction f_{screw}.

$$f_{screw} = 1 - f_{edge} = \frac{q_{exp} - q_{edge}}{q_{screw} - q_{edge}} \quad (7)$$

Next, the modified Warren-Averbach method[3] is used to derive the dislocation density, crystallite size, and dislocation arrangement parameter. The modified Warren-Averbach equation is expressed by Equation (9), which incorporates the relationship between lattice distortion and dislocations (8)[9, 10] into the Warren-Averbach equation.

$$\langle\varepsilon_L^2\rangle \cong \frac{\rho\bar{C}_{hkl}b^2}{4\pi}\ln\left(\frac{R_e}{L}\right) \quad (8)$$

$$\ln A(L) \cong \ln A^S(L) - \rho B^* L^2 \ln\left(\frac{R_e}{L}\right)\left(K^2\bar{C}_{hkl}\right) + O\left(K^2\bar{C}_{hkl}\right)^2 \quad (9)$$

Here, $\langle\varepsilon_L^2\rangle$ is the mean square strain, and L is the Fourier length. $L=na_3$, where n is an integer and $a_3=\lambda/[2(\sin\theta_2-\sin\theta_1)]$. θ_1 and θ_2 are the start and end angles of the diffraction peak, respectively, and λ is the X-ray wavelength. Furthermore, $A(L)$ is the real part of the Fourier coefficient of the measured peak, $A^S(L)$ is the Fourier coefficient originating from the crystallite size, O is the higher-order term, and $B^*=\pi b^2/2$.

The modified Warren-Averbach equation is a quadratic function with $K^2\bar{C}_{hkl}$ as a variable. Therefore, plotting $\ln A(L)$ against $K^2\bar{C}_{hkl}$ yields the value of $\ln A^S(L)$ related to crystallite size from the y-intercept for various L values, and the value of $-\rho B^* L^2\ln(R_e/L)$ related to dislocation density from the linear coefficient. Setting $-\rho B^* L^2\ln(R_e/L)=X(L)$ and dividing by L^2 yields Equation (10). This equation is a linear function with variable $\ln L$. Plotting $X(L)/L^2$ against $\ln L$ allows the value of $-\rho B^*=-\rho(\pi b^2/2)$ to be determined from the slope of the line, thereby determining the dislocation density ρ.[5]

$$\frac{X(L)}{L^2} = \rho B^*\ln\left(\frac{R_e}{L}\right) = \rho B^*\ln R_e - \rho B^*\ln L \quad (10)$$

Simultaneously, dividing the value of $\rho B^*\ln R_e$ obtained from the y-intercept by ρB^* determines R_e. Substituting this into Equation (11) yields the dislocation arrangement parameter M^*. Here, $R_e^*=R_e/\exp 2$.

$$M^* = R_e^*\sqrt{\rho} \quad (11)$$

Furthermore, the x-intercept of the straight line determined from the initial slope near $L=0$ when plotting $A^S(L)$ versus L defines the area-weighted average crystallite size $\langle t\rangle_{area}$.

For a detailed explanation of the fundamental relationship between size-strain distribution and diffraction profile shape, as well as the XLPA methods based on the classical Williamson-Hall method/Warren-Averbach method and the modified Williamson-Hall/modified Warren-Averbach methods, please refer to Reference 11).

3. Results and Discussion

3.1 Analysis of flat specimens

Figure 2 shows the analysis results for flat plate samples milled for different durations, measured using the B-B method and the micro-focus method.

For dislocation density and crystallite size, both methods yielded

nearly identical values, though values from the micro-focus method tended to be slightly higher. For the dislocation arrangement parameter M^*, both methods produced close values. Regarding the fraction of screw dislocations, values for 0 hours and 1 hour were similar, with a slight difference appearing at 6 hours.

First, we examine the change in the fraction of screw dislocations. Dislocation theory states that positive and negative dislocations annihilate each other when they meet on the same slip plane. Compared to edge dislocations, which cannot move to different slip planes unless at high temperatures, screw dislocations can easily move to different slip planes via cross-slip. Therefore, the probability of screw dislocations encountering each other is higher, making annihilation more likely. Consequently, when dislocation density increases in a non-high-temperature environment, the fraction of screw dislocations tends to decrease. In Fig. 2(d), the micro-focus method shows a gradual decrease in the fraction of screw dislocations with increasing dislocation density, consistent with dislocation theory. Khatirkar et al.[12] investigated the relationship between milling time and the fraction of screw dislocations using the modified Williamson-Hall method, after intensively processing iron powder in a planetary ball mill and performing XRD measurements using the B-B method. According to their results, after 4 hours of milling, screw dislocations were the main component. After 8, 12, and 16 hours, screw and edge dislocations were roughly equal in fraction. After 20 hours, screw dislocations again became the main component. Although no discussion of this is provided, the use of heavy-duty milling (planetary ball mill) likely heated the iron powder sample, creating an environment conducive to pair annihilation of edge dislocations, potentially increasing the relative fraction of screw dislocations. The difference from Khatirkar et al.'s results is likely due to this study using a rotating ball mill for light milling under near-ambient conditions.

Next, we consider changes in dislocation arrangement parameters. Individual dislocations that cannot annihilate become stable, arranging themselves so their surrounding strain fields cancel each other out. Stable pairs of dislocations are called dislocation dipoles. The microstructure stabilizes into regions with high dislocation density walls and relatively low dislocation density areas, known as dislocation cells. When individual dislocations are randomly arranged without interaction, the radius R_e^* of the strain field around a dislocation line is much larger than the average dislocation distance $1/\sqrt{\rho}$. This state can be expressed as $R_e^* \gg 1/\sqrt{\rho}$, and rearranging the equation yields $R_e^*\sqrt{\rho}(=M^*) \gg 1$. Conversely, when dislocation interactions are strong (e.g., when dislocation dipoles or dislocation cells form), opposite-sign dislocations are close to each other and strain fields are strongly screened, making R_e^* smaller than $1/\sqrt{\rho}$. This state is $R_e^* \ll 1/\sqrt{\rho}$, so $R_e^*\sqrt{\rho}(=M^*) \ll 1$.[13, 14] In this experimental result, since $M^* \ll 1$ before and after milling, dislocation dipoles likely existed prior to milling, and milling increased the number of randomly arranged dislocations.

Next, we examine why the dislocation density and crystallite size obtained using the micro-focus method were slightly higher than those obtained using the B-B method, and why the fraction of screw dislocations differed for the 6-hour ball milling case. The reason for this difference is not clear, but it is possible that the micro-focus method provided a more appropriate analysis than the B-B

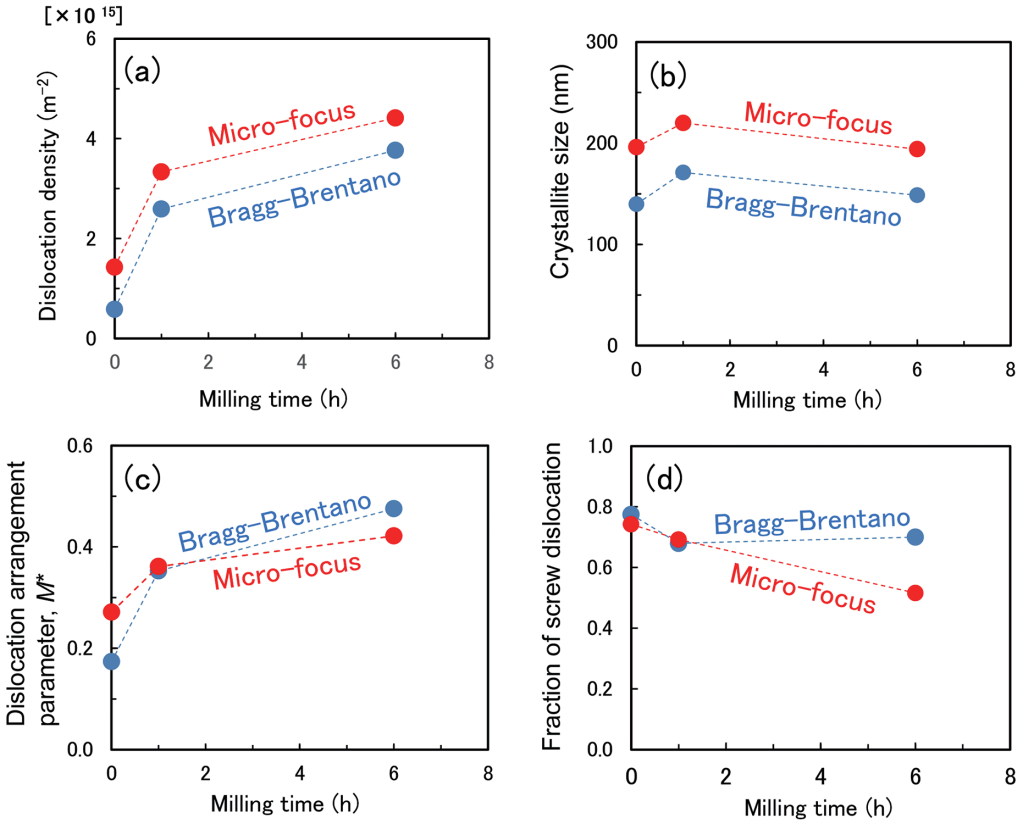

Fig. 2 Changes in (a) dislocation density, (b) crystallite size, (c) dislocation arrangement parameter M^*, and (d) fraction of screw dislocation as a function of milling time. ● Bragg-Brentano geometry, ● Micro-focus geometry

method. The first piece of evidence is the peak profile observed when measuring LaB_6 by XRD. The ideal peak profile for XRD measurements of crystals without lattice distortion, such as LaB_6, is the Laue function type, which approximates a Gaussian function. The line profile of LaB_6 obtained by the B-B method exhibits a Voigt function shape, whereas the micro-focus method yields a Gaussian function shape. This suggests the micro-focus method may be more likely to produce ideal peak profiles. The second piece of evidence is that the micro-focus method revealed a trend consistent with dislocation theory: the fraction of screw dislocations decreases with increasing milling time. However, it remains unclear whether these findings apply equally to other materials analyzed, necessitating further detailed investigation.

3.2 Analysis of curved specimens

3.2.1 Simulation of X-ray peak profiles for curved specimens

Flat and curved specimens molded from iron powder milled for one hour were measured using the micro-focus method and the B-B method to compare the α-Fe 110 peak profiles. The $K\alpha_2$ line profile was suppressed using the Rachinger method. **Figure 3** (a) shows the peak profiles measured using the micro-focus method. Both the flat sample (Flat) and the curved samples (R5, R10, R15) exhibit left-right symmetry, allowing fitting with symmetric functions such as Voigt or Lorentz. There is also little change in the FWHM. In contrast, Fig. 3 (b) shows peak profiles measured using the B-B method. While the flat sample (Flat) exhibits symmetry, the curved samples (R5, R10, R15) are asymmetrical, with the FWHM broadening by nearly a factor of two. Therefore, measuring curved samples using the B-B method yields erroneous FWHM values.

The left-right asymmetry in the peak profiles of curved samples is thought to be related to the non-uniform height of the measurement surface. Therefore, experiments were conducted to investigate the relationship between the measurement surface height and the peak profile. Figure 3 (c) shows the α-Fe 110 peak profiles obtained by XRD measurement using the B-B method. The measurement surface of the flat plate sample, formed from iron powder milled for one hour and molded with resin, was shifted 0.5 mm at a time in the -y direction (Fig. 1) relative to the goniometer center. As the measurement surface height decreased (shifted in the -y direction of Fig. 1), the peak profile shifted toward lower angles while maintaining its FWHM, and the diffraction intensity decreased monotonically. This suggests that the peak profile of the curved sample is likely composed of multiple peak profiles integrated together, as shown in Fig. 3 (c). Therefore, we calculated the peak profile shift amount based on the height deviation of the measurement plane for the curved sample and simulated the asymmetric peak profile of the curved sample by integrating multiple peak profiles. For details of the simulation, refer to Reference 15). As a result, the profiles shown in Fig. 3 (d) were obtained from the simulation, exhibiting shapes nearly identical to the measured profiles shown in Fig. 3 (b). This clearly demonstrated that the height deviation of the measurement surface causes the peak profile of the curved sample to become asymmetric. Furthermore, this simulation enabled the calculation and prediction of the curvature level at which the peak profile change is minimal when measuring curved samples using the B-B method, without the need to fabricate and measure curved samples.

Next, to investigate the relationship between the sample curvature and the X-ray irradiation width, simulations were performed by varying the X-ray irradiation width L in the direction perpendicular to the X-ray propagation direction (the x-direction in Fig. 1). **Figure 4** shows the relationship between the symmetry S of the α-Fe 110 diffraction peak profile and the sample radius R for simulations performed with X-ray irradiation widths L=1, 5, and 15 mm.

The vertical axis represents symmetry $S=FWHM_L/FWHM_R$. Here, the $FWHM_L$ corresponds to the left half of the peak profile, and the $FWHM_R$ corresponds to the right half. When the peak profile is bilaterally symmetric, the value of S is 1. When measuring highly curved samples using the B-B method, the peak profile becomes asymmetric for both X-ray irradiation widths L=5 mm and L=15 mm. However, it is found that a bilaterally symmetric peak profile is obtained regardless of curvature when L=1 mm.

3.2.2 Line profile analysis of curved samples

Using the micro-focus method with a 0.2 mm diameter collimator, θ-2θ measurements were performed on the hemicylindrical curved samples shown in Table 1. X-rays passing through the 0.2 mm diameter collimator diverge, resulting in an actual X-ray irradi-

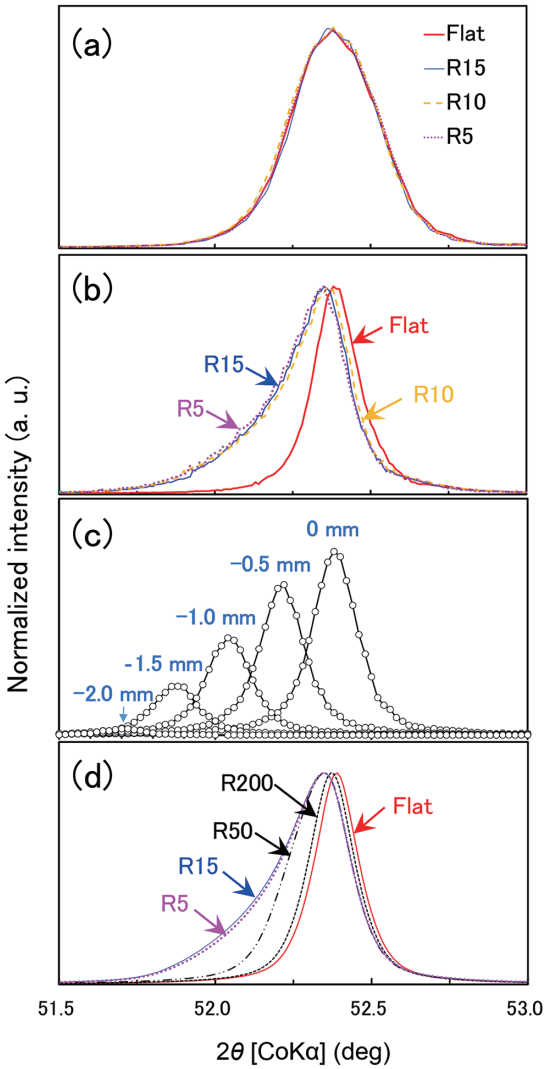

Fig. 3 X-ray peak profiles of 110 reflection for 1 hour milled Fe samples
(a) measured by the Micro-focus method
(b) measured by the Bragg-Brentano method
(c) measured by the Bragg-Brentano method with various heights
(d) simulated by the Bragg-Brentano method with various radii

ation width of approximately 1 mm perpendicular to the X-ray propagation direction (the x-direction in Fig. 1) at the sample surface. **Figure 5** shows (a) dislocation density, (b) crystallite size, (c) dislocation arrangement parameter, and (d) fraction of screw dislocations for curved samples with varying radii R.

The trend of dislocation density increasing with milling time was observed for R10 and R15, but not for $R^{-1}=0.2$ (R5).

Focusing only on the milled samples (1 hour and 6 hours), the trend in crystallite size with increasing milling time does not deviate significantly except for $R^{-1}=0.2$ (R5).

The dislocation arrangement parameter M^* showed similar trends except for $R^{-1}\approx0.07$ (R15).

The trend in the fraction of screw dislocations with increasing milling time shows no significant change when focusing only on the milled samples (1 hour and 6 hours).

Therefore, the applicability limit for evaluating dislocation density in curved samples using 1 mm-wide X-rays is considered to be up to R10. The large variation in values for unmilled samples is estimated to be due to the low angular resolution of the micro-focus method, which makes the peak width too narrow in unmilled samples, making it difficult to evaluate the FWHM of the profile originating from the sample. The fluctuation in values such as dislocation density and crystallite size with changes in sample radius R is estimated to be due to the low-angle diffraction peaks being susceptible to height shifts, which also affected the peak profiles[15)]

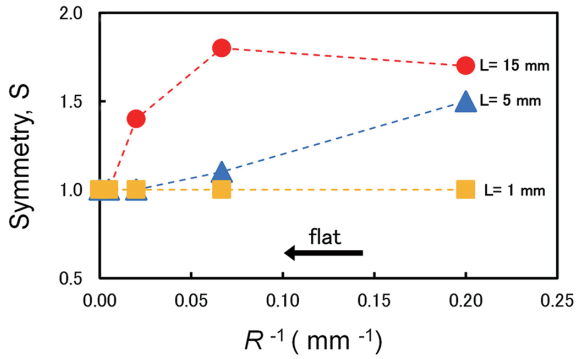

Fig. 4 Relationship between asymmetry of 110 peak profile and radius of sample

4. Conclusion

XRD measurements were performed on iron powder molded into flat plates and cylinders using both the B-B method and the micro-focus method, and X-ray line profile analysis was conducted to investigate the limitations of application to micro-regions and curved materials.

As a result, it was found that the micro-focus method and the B-B method yield nearly identical dislocation densities and crystallite sizes for flat specimens. When measuring curved specimens using the B-B method, it became clear that height differences in the specimen measurement surface cause asymmetric peak profiles. It was also found that setting the X-ray irradiation width to 1 mm yields symmetric peak profiles. Furthermore, it was found that using the micro-focus method with an X-ray irradiation width of 1 mm enables dislocation density measurement if the radius of specimen is 10 mm or larger.

References

1) Williamson, G.K. et al.: Acta Metal. 1 (1), 22 (1953)
2) Warren, B.E. et al.: J. Appl. Phys. 21 (6), 595 (1950)
3) Ungár, T. et al.: Appl. Phys. Lett. 69 (21), 3173 (1996)
4) Ungár, T. et al.: Phys. Status Solidi. 171 (2), 425 (1999)
5) Ungár, T. et al.: Acta Mater. 46 (10), 3693 (1998)

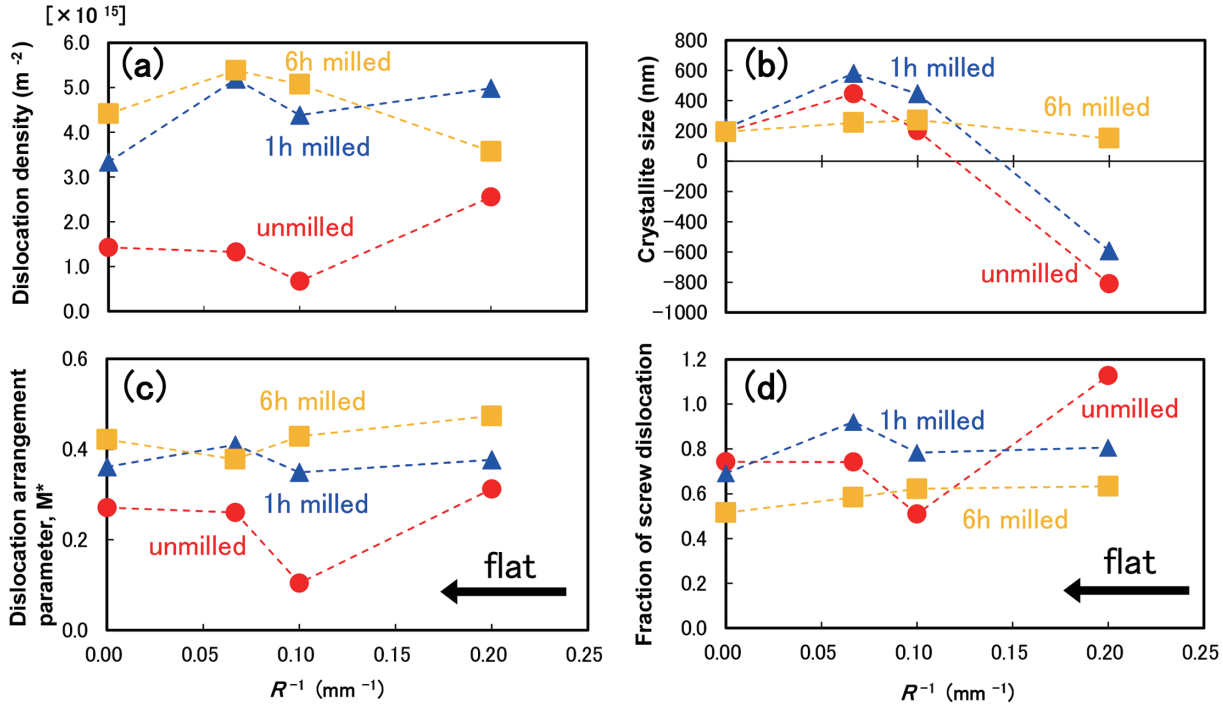

Fig. 5 Changes in (a) dislocation density, (b) crystallite size, (c) dislocation arrangement parameter M^*, and (d) fraction of screw dislocation as a function of R^{-1}. ●: unmilled, ▲: 1h milled, ■: 6h milled

6) Tomota, Y. et al.: Tetsu-to-Hagané. 103 (2), 73 (2017)
7) Rachinger, W.A.: J. Sci. Instrum. 25 (7), 254 (1948)
8) Borbély, A. et al.: J. Appl. Crystallogr. 36 (1), 160 (2003)
9) Krivoglas, M.A.: Theory of X-Ray and Thermal Neutron Scattering by Real Crystals. New York, Plenum Press, 1969
10) Simmons, J.A. et al.: Fundamental Aspects of Dislocation Theory. Spec. Publ. No. 317. Vol. II. Washington DC, Nat. Bur. Stand. (US), 1970, 1195p
11) Ito, A.: Fundamental Study on Dislocation Characterization of Steel Material by X-Ray Diffraction. Tokyo City University. Doctoral Dissertation (Engineering). No. 184. 2023-03-19. Chapter 2. p.50–67 (in Japanese)
12) Khatirkar, R.K. et al.: Mater. Chem. Phys. 123 (1), 247 (2010)
13) Wilkens, M.: Phys. Status Solidi A. 2 (2), 359 (1970)
14) Ribárik, G. et al.: Crystals. 10 (7), 623 (2020)
15) Itoh, A. et al.: Tetsu-to-Hagané. 109 (4), 267 (2023)

Atsuhiro ITOH
Dr. Eng., Senior Manager
Structure Characterization Dept.
Physical Characterization Solution Div.
R&D Supporting Unit
Nippon Steel Technology Co., Ltd.
20-1 Shintomi, Futtsu City, Chiba Pref. 293-0011

Muneyuki IMAFUKU
Dr. Eng., Professor
Department of Mechanical Systems Engineering
Tokyo City University